A Three-Dimensional Finite Element Method for a Nonisothermal Aluminum Flat Strip Rolling Process

Z.-C. Lin and C.-C. Shen

The purpose of this study is to develop a three-dimensional coupled thermo-elastic-plastic finite element model of nonisothermal rolling and analyze the strip curvature caused by the difference in the heat transfer boundary conditions of the upper and lower rollers. The difference in the rotation speed between the upper and lower rollers was utilized in an attempt to correct the aforementioned curvature in hot rolling due to unsymmetrical cooling conditions. In addition, the changes in shape, temperature field, and strain field of the strip during the various stages were analyzed and can be used to obtain the lateral plastic flow of the strip. As for the aspect of heat transfer, the various possible boundary conditions in the actual hot rolling were considered, which include the convection boiling of the air and water, and the radiation loss. Then, the three-dimensional finite difference heat transfer equation is derived according to the concept of heat balance. As for the determination of the direction of tangential friction force, this study also developed a modification algorithm to adjust to the three-dimensional rolling process. After a comparison with the experimental data in Ref 8 and 15, and the simulated temperature distribution in Ref 17, the partial results obtained from the computation by the numerical analytical model verify that the theoretical model and computer programs established in this study are reasonable. This study shows that hot rolling can greatly reduce the rolling force and strain rate with the early appearance of plastic deformation, and the distribution of temperature field is basically affected by the heat transfer boundary conditions. However, unsymmetrical heat transfer boundary conditions will cause unsymmetrical rolling forces of the upper and lower rollers and cause strip curvature; this condition can be corrected by the difference in the rotation speed of the rollers.

Keywords

coupled thermo-elastic-plastic, finite element model, nonisothermal rolling

1. Introduction

RAPID development in the research of metal rolling has occurred in recent years. The primary goal of plastic deformation analysis is to estimate the partial strain rate, strain, stress, and temperature of the strip during the rolling process. The conventional plastic dynamics theory provided enough equations to obtain the values of stress and strain. It is still lacking in the area of dynamics during the formation process, especially for the complicated metal rolling formation. It is now impossible to obtain the accurate solution for metal rolling by means of equations. Along with the advancement of computer hardware and software, the analysis of metal formation must be done with a numerical method. In this study, the finite element numerical method is used to analyze the behavior of three-dimensional, nonisothermal elastic-plastic rolling deformation of aluminum strips. The plastic deformation and the changes in temperature were also explored. In this study, the hexahedron element was used as the three-dimensional finite element and divided into five 4-node tetrahedral elements. The behavior of rolling formation of aluminum strips under a nonisothermal condition is also studied. The difference in the rotation speed of the upper and lower rollers in unsymmetrical rolling was used to correct the phenomenon of vertical curvature due to the nonisothermal condition.

In 1982, Li and Kobayashi (Ref 1) used finite elements and the small deformation theory to analyze plastic steel materials. They analyzed the velocity field inside the deformation area and the distribution of stress and the distribution of pressure inside the contact arch during the cold rolling of plates, without considering the temperature effects. In 1988, Shivpuri et al. (Ref 2) studied the strip curvature caused by the difference in the rotation speed of the upper and lower rollers in unsymmetrical rolling. They used the two-dimensional elastic material model, without considering the temperature effects. In 1989, Chen et al. (Ref 3) conducted a study that conformed with Newton's law of motion and hypothesized that within the same time increment the rolling process was a quasi-static state model. They used the dynamic relaxation method in the finite difference method to solve this problem. The material was hypothesized as elastic-plastic, and the strain rate and the temperature effects were not considered. In another study by Zienkiewicz et al. (Ref 4) in 1981, the steady-state hot rolling as a result of the softening effects of the temperature was considered. They used the Galerkin weighted residuals method to solve the force equilibrium equation and the heat balance equation. They also used the iteration method to solve these two coupled finite element equations. However, if the same method is used to solve the nonsteady state rolling, then during each time increment the temperature field and velocity field can only be solved by going through several rounds of iteration. In addition, they assumed the material to be of plastic steel.

Other literature results are concerned with the problem of heat transfer in rolling. In 1984, Tseng (Ref 5, 6) analyzed the strip temperature during two-dimensional steady-state rolling.

Z.C. Lin, Professor, Department of Mechanical Engineering, National Taiwan Institute of Technology, Taipei, 106, Taiwan, Republic of China; **C.C. Shen,** Graduate Assistant, Department of Mechanical Engineering, National Taiwan Institute of Technology, Taipei, 106, Taiwan, Republic of China.

The temperature field of the rollers and strip were analyzed comprehensively, but the temperature field of three-dimensional strips was not explored. In 1986, Devadas and Samarasekera (Ref 7) focused on the actual conditions of continuous hot rolling and analyzed the temperature of the strip and rollers by a one-dimensional transient heat transfer finite difference method.

The research in this area has so far remained mostly two-dimensional analysis or without the considerations of the temperature effects and the problem of boundary heat transfer. The purpose of this study is to develop the theoretical model and computer programs of a three-dimensional coupled thermo-elastic-plastic large deformation finite element analysis for aluminum strip rolling, with the consideration of the heat transfer boundary conditions during actual rolling. The finite difference model was used to calculate the temperature of each element to make up for the related data from the rolling formation process, which are quite difficult to obtain. Finally, a simulation was conducted using aluminum strips.

First, cold rolling was conducted to analyze the rolling force and the average rolling torque, which was then compared with the experimental data by Al-Salehi et al. (Ref 8). The comparison between the present results and the simulated temperature distribution by Dawson (Ref 16) indicates identical temperature distributions and verifies the theoretical model and computer program established in this study. The roller is assumed to be rigid in this paper, which means there is no roller deformation. The average rolling torque is derived by directly calculating the rolling force of the roller in the tangential direction and then multiplying by a roller radius of 79.375 mm. Then the three-dimensional non-isothermal hot rolling was analyzed, and a simulation was implemented to use the difference in the rotation speed of the upper and lower rollers to prevent the vertical curvature of the strip. This study shows that hot rolling can greatly reduce rolling force and strain rate with the early appearance of plastic deformation, and the distribution of temperature field is basically affected by the heat transfer boundary conditions. However, unsymmetrical heat transfer boundary conditions will cause unsymmetrical rolling forces of the upper and lower rollers and cause strip curvature, but the above condition can be corrected by the difference in the rotation speed of the rollers.

2. The Governing Equation of the Three-Dimensional Thermo-Elastic-Plastic Finite Element

If the plastic strain increment $\{d\varepsilon^p\}$ can be derived from plastic potential f and the Prandtl-Reuss flow rule, then the plastic potential f is the same as the yield criterion. When the stress state of the element within the workpiece falls exactly on the yielding surface, its differential equation should satisfy (Ref 9):

$$\{\dot{\sigma}\} = [D^{ep}](\{\dot{\varepsilon}\} - \{\dot{\varepsilon}^t\}) + \frac{d}{dt}\left(\frac{[D^e]\left\{\frac{\partial f}{\partial \sigma}\right\}\left(\frac{\partial R}{\partial \bar{\varepsilon}}\dot{\bar{\varepsilon}} + \frac{\partial R}{\partial T}dT\right)}{H' + \left\{\frac{\partial f}{\partial \sigma}\right\}^T [D^e]\left\{\frac{\partial f}{\partial \sigma}\right\}}\right) \quad \text{(Eq 1)}$$

where

$$[D^{ep}] = [D^e] - \frac{[D^e]\left\{\frac{\partial f}{\partial \sigma}\right\}\left\{\frac{\partial f}{\partial \sigma}\right\}^T [D^e]}{H' + \left\{\frac{\partial f}{\partial \sigma}\right\}^T [D^e]\left\{\frac{\partial f}{\partial \sigma}\right\}}$$

$f(\sigma_{ij})$ is the positive function of the stress. $R(\bar{\varepsilon}^p, \dot{\bar{\varepsilon}}, T)$ is the area of the yielding surface.

Since the element principal axis had a spinning phenomenon during metal forming, this study selected the Jaumann rate of Euler stress $[\tilde{\sigma}]$ as the stress rate of the constitution Eq 1. Thus,

$$\{\tilde{\dot{\sigma}}\} = [D^{ep}](\{\dot{\varepsilon}\} - \{\dot{\varepsilon}^t\}) + \frac{d}{dt}\left(\frac{[D^e]\left\{\frac{\partial f}{\partial \sigma}\right\}\left(\frac{\partial R}{\partial \bar{\varepsilon}}\dot{\bar{\varepsilon}} + \frac{\partial R}{\partial T}dT\right)}{H' + \left\{\frac{\partial f}{\partial \sigma}\right\}^T [D^e]\left\{\frac{\partial f}{\partial \sigma}\right\}}\right) \quad \text{(Eq 2)}$$

Without considering the effects of body force, the equilibrium equation of the principle of virtual work for the large deformation-large strain should be:

$$\int_v \{\delta\dot{e}\}^T \{\dot{\sigma}_1\}\, dv = \int_s \{\delta\dot{u}\}^T \{\dot{\bar{f}}_0\} ds \quad \text{(Eq 3)}$$

where $\dot{u}$ is deformation rate velocity of the body, $\dot{\sigma}_1$ is Lagrangian stress rate, $\dot{\bar{f}}_0$ is the traction variation rate according to present area, and $\dot{e}$ is velocity gradient of the body.

If $\dot{\rho}/\rho$ is taken to be zero to satisfy the material incompressibility, then the finite element formulation with the large deformation-large strain stiffness is derived as:

$$([K_{ep}] + [K_G])\{\dot{d}\} = \int_v [B_\varepsilon]^T [D^{ep}] \{\dot{\varepsilon}^t\}\, dv - \int_v [B_\varepsilon]^T \{\dot{R}_{\bar{\varepsilon}T}\}\, dv + \{\dot{F}_0\} \quad \text{(Eq 4)}$$

where

$$[K_{ep}] = \Sigma_{allelement} \int_v [B_\varepsilon]^T [D^{ep}] [B_\varepsilon]\, dv$$

$$[K_G] = \Sigma_{\text{allelement}} \int_v [B_e]^T [D^{ep}] [B_e] \, dv$$

$$\{\dot{F}_0\} = \Sigma_{\text{allelement}} \int_s [N]^T \{\dot{f}_0\} \, ds$$

$$\{\dot{R}_{\bar{\varepsilon}T}\} = \frac{d}{dt}\left(\frac{2\bar{\sigma}}{3S_0}\{S\}\left(\frac{\partial R}{\partial \bar{\varepsilon}} d\bar{\varepsilon} + \frac{\partial R}{\partial T} dT\right)\right)$$

$[K_{ep}]$ = elastic-plastic element stiffness matrix

$[K_G]$ = geometric stiffness matrix

$\{\dot{F}_0\}$ = variation rate of node force

The usual derivation of strain rate has been the one-order derivation. However, this study followed the concept of a two-order strain rate and used the Lin (Ref 9) strain rate equation and strain rate error value e as the rule for determining convergence.

3. The Algorithm for Determining the Direction of Friction

Since the contact region between the roller and the strip is represented with a local coordinate, the ($[K_{ep}] + [K_G]$) in Eq 4 has to be appropriately modified on the coordinates.

$$\begin{bmatrix} \bar{K}_{ss} & \bar{K}_{si} \\ K_{is} & K_{ii} \end{bmatrix} \begin{Bmatrix} \dot{d}_l^s \\ \cdots \\ \dot{d}_G^i \end{Bmatrix} = \begin{Bmatrix} \dot{F}_\xi \\ \dot{F}_\eta \\ \dot{F}_\zeta \\ \cdots \end{Bmatrix} + \int_v [B_\varepsilon]^T [D^{ep}] \{\dot{\varepsilon}^t\} \, dv - \int_v [B_\varepsilon]^T \{\dot{R}_{\bar{\varepsilon}T}\} \, dv \qquad \text{(Eq 5)}$$

where

$$[\bar{K}_{ss}] = [T_n]^T [K_{ep}^{ss} + K_G^{ss}] [T_n]$$

$$[\bar{K}_{si}] = [T_n]^T [K_{ep}^{si} + K_G^{si}]$$

$$[\bar{K}_{is}] = [K_{ep}^{is} + K_G^{is}] [T_n]$$

$$[\bar{K}_{ii}] = [K_{ep}^{ii} + K_G^{ii}]$$

Here, subscript s represents the node on the contact surface between the roller and the strip, and subscript i is inner node of the strip. The l and G refer to the physical property based on the local and global coordinate system. $\dot{F}_\xi$ represents the ξ directional tangent load increment of the contact node between the strip and the roller. $\dot{F}_\eta$ represents the normal load increment of the contact node between the strip and the roller. $\dot{F}_\zeta$ represents the ζ directional tangent load increment of the contact node between the strip and the roller. $[T_n]$ is the coordinate transfer matrix; i.e., $\{\dot{d}_G^s\} = [T_n] \{\dot{d}_l^s\}$. Also shown in Fig. 1, this equation is as follows:

$$\{\dot{d}_G^s\} = \begin{Bmatrix} \dot{d}_{Gx}^s \\ \dot{d}_{Gy}^s \\ \dot{d}_{Gz}^s \end{Bmatrix} = \begin{bmatrix} \cos\theta & -\sin\theta & 0 \\ \sin\theta & \cos\theta & 0 \\ 0 & 0 & 1 \end{bmatrix} \begin{Bmatrix} \dot{d}_\xi^s \\ \dot{d}_\eta^s \\ \dot{d}_\zeta^s \end{Bmatrix} \qquad \text{(Eq 6)}$$

For rigid body rollers, the velocity of the normal direction of the contact node between the strip and the roller equals zero. As for the tangent direction, the roller and strip has a relative velocity; therefore, $\{\dot{d}_l\}$ can be written as:

$$\{\dot{d}_l\}_{1\times 12} = \{\Delta\dot{d}_{1\xi} + \dot{d}_\xi^R \;\; 0 \;\; \Delta\dot{d}_{1\zeta} \;\; \Delta\dot{d}_{2\xi} + \dot{d}_\xi^R \;\; 0 \;\; \Delta\dot{d}_{1\zeta} \;\; \Delta\dot{d}_{3\xi} + \dot{d}_\xi^R \;\; 0 \;\; \Delta\dot{d}_{3\zeta} \;\; \dot{d}_{4x} \;\; \dot{d}_{4y} \;\; \dot{d}_{4z}\}$$

where $\Delta\dot{d}_{1\xi}$, $\Delta\dot{d}_{2\xi}$, and $\Delta\dot{d}_{3\xi}$ are the relative velocity between the strip and the roller in the tangent direction, ξ. $\dot{d}_\xi^R$ is the tangent velocity of the roller surface. $\Delta\dot{d}_{1\zeta}$, $\Delta\dot{d}_{2\zeta}$, and $\Delta\dot{d}_{3\zeta}$ are the relative velocity between the strip and the roller in the perpendicular direction ζ of the tangent and normal directions.

As far as the contact node between the surface of the strip and the roller is concerned, Coulomb's friction rule is used $|\vec{F}_\xi + \vec{F}_\zeta| = |\mu\vec{F}_\eta|$. The force on the node within the strip is equilibrium to zero; therefore,

$$\{\dot{F}_l(d)\}_{1\times 12} = \{A_1\dot{F}_{1\eta} \;\; \dot{F}_{1\eta} \;\; B_1\dot{F}_{1\eta} \;\; A_2\dot{F}_{2\eta} \;\; \dot{F}_{2\eta} \;\; B_2\dot{F}_{1\eta} \;\; A_3\dot{F}_{3\eta} \;\; \dot{F}_{3\eta} \;\; B_3\dot{F}_{1\eta} \;\; 0 \;\; 0 \;\; 0\} \qquad \text{(Eq 7)}$$

where

$$A_i = \frac{1}{\sqrt{1 + \tan^2\phi_i}} |\mu^0|$$

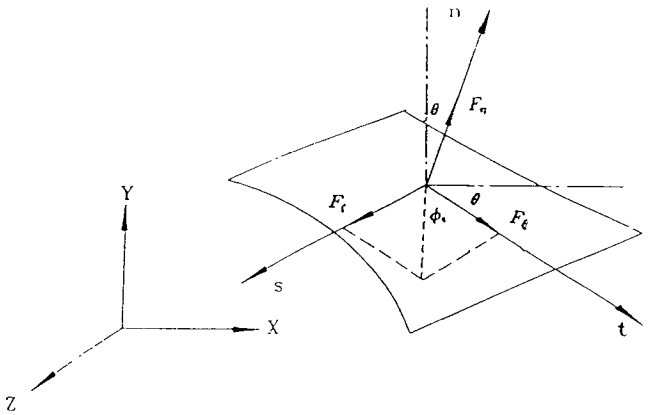

Fig. 1 Relationship between global and local coordinates

$$B_i = \frac{\tan \varphi_i}{\sqrt{1 + \tan^2 \phi_i}} |\mu^0|$$

$$\tan \phi_i = \dot{F}_{i\zeta} / \dot{F}_{i\xi}, \quad i = 1, 2, 3$$

For the direction of friction force, see Fig. 2. The following definitions match the direction of real friction force with the local coordinate. The distance between the upper roller entrance and the neutral point is $\mu^0 = -\mu$. The distance between the upper roller neutral point and the exit is $\mu^0 = +\mu$. The distance between the lower roller entrance and the neutral point is $\mu^0 = +\mu$. The distance between the lower roller neutral point and the exit is $\mu^0 = -\mu$.

Using the value of this strain field and the assumption of no volume change in the plastic deformation $\Delta\varepsilon_x + \Delta\varepsilon_y + \Delta\varepsilon_z = 0$, we selected $|\Delta\varepsilon_x + \Delta\varepsilon_y + \Delta\varepsilon_z| < 10^{-6}$ as the basis to decide whether tan ϕ_i needs to be modified. The steps for determining the tan ϕ_i are as follows:

Step 1: At the beginning of the simulation, give the contact node i an initial value of tan ϕ_i.

Step 2: After calculation by a computer program, the strain increment $\{\Delta\varepsilon\}$ is derived.

Step 3: If $|\Delta\varepsilon_x + \Delta\varepsilon_y + \Delta\varepsilon_z| > 10^{-6}$, then modify tan ϕ_i and repeat Step 2.

Step 4: If $|\Delta\varepsilon_x + \Delta\varepsilon_y + \Delta\varepsilon_z| < 10^{-6}$, then use this tan ϕ_i as the initial value for the next stage.

Step 5: Repeat the above steps until the simulation is finished.

4. The Decisive Algorithm of the Neutral Point

The neutral point is the point at which the tangent velocities of the roller and strip are the same. The direction of material flow and friction force is opposite between the neutral point and the exit. During rolling, the surface nodes of the strip will pass by the roller one after the other. To determine the direction of friction, decide whether the node is located between the entrance and the neutral point or between the neutral point and the exit.

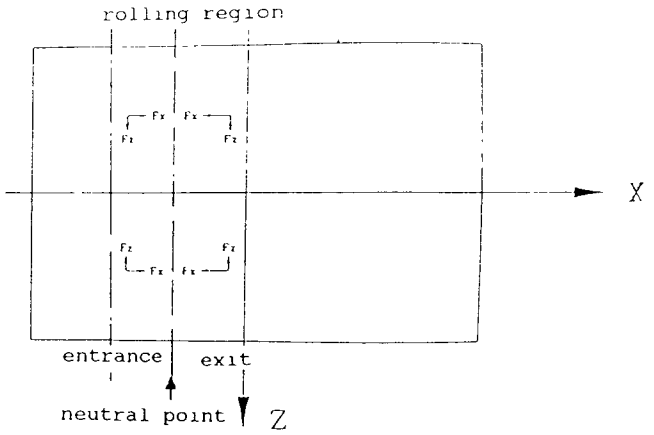

Fig. 2 Direction of friction force of the roller rolling on the strip surface

To determine if the neutral point will still be the neutral point at time t, first determine if at time t, $|\vec{F}^t_\xi + \vec{F}^t_\zeta| \geq |\mu \vec{F}^t_\eta|$ and $F^t_\xi < 0$. Then take the next surface node as the neutral point at time $t + \Delta t$ and change the boundary condition of that node. If $|\vec{F}^t_\xi + \vec{F}^t_\zeta| < |\mu \vec{F}^t_\eta|$, then proceed without changing the boundary condition of that node.

5. Heat Transfer Model of Strip

5.1 *Inner Element*

As shown in Fig. 3, the control volume passing through element C or the heat source in such a control volume can obtain its finite difference model from the central difference between the appropriate space and time differentiation. Based on the heat balance of the element C control volume, it is written as:

$$\dot{q}_t + \dot{q}_W + \dot{q}_F + \dot{q}_S = \dot{q}_E + \dot{q}_B + \dot{q}_N + \dot{q}_m + \dot{q}''' \qquad \text{(Eq 8)}$$

where,

$$\dot{q}m = \rho c u(x) \frac{\partial T}{\partial X} V_e = \rho c u(x) \frac{T^i_{W'} - T^i_{E'}}{X_c} V_e$$

is the energy variation rate within the elements along with changes in position.

$$\dot{q}_t = \rho c \frac{\partial T}{\partial t} V_e = \rho c \frac{T^{i+1}_C - T^i_C}{\Delta t} V_e$$

is the energy variation rate within the elements along with changes in time.

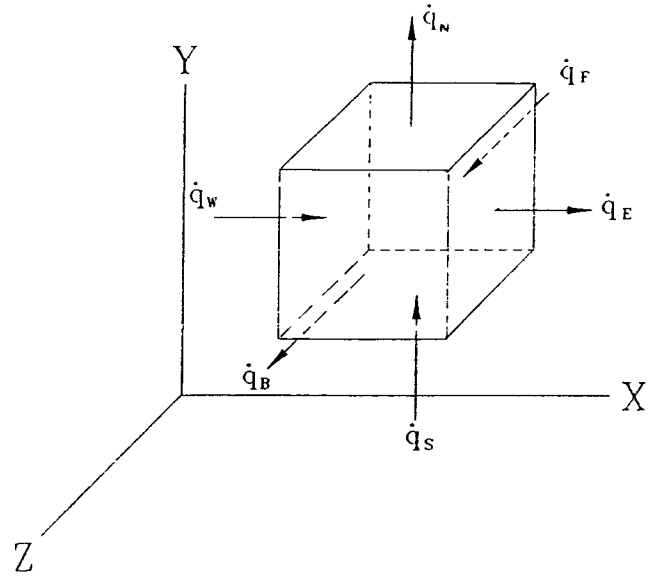

Fig. 3 Energy balance of control-volume element

$$\dot{q}''' = \eta_p \, \bar{\sigma} \, \dot{\bar{\varepsilon}} \, V_e$$

is the plastic deformation heat of the elements.

$$\dot{q}_{W,F,S,E,B,N} = -KA \frac{\partial T}{\partial n}$$

is the six heat transfer heat of the three-dimensional elements based on Fourier's law.

It can be rearranged as:

$$T^{i+1} =$$
$$T_C^i \left[1 - \alpha \Delta t \left(\frac{1}{I_E E_x} + \frac{1}{I_B B_z} + \frac{1}{I_N N_y} + \frac{1}{I_W W_x} + \frac{1}{I_F F_z} + \frac{1}{I_S S_y} \right) \right]$$
$$+ \alpha \Delta t \left(\frac{T_E^i}{I_E E_x} + \frac{T_B^i}{I_B B_z} + \frac{T_N^i}{I_N N_y} + \frac{T_W^i}{I_W W_x} + \frac{T_F^i}{I_F F_z} + \frac{T_S^i}{I_S S_y} \right)$$
$$+ u(x) \Delta t \frac{T_{W'}^i - T_{E'}^i}{X_c} + \frac{\Delta \dot{q}'''}{\rho c V_e} \qquad \text{(Eq 9)}$$

where A_W, A_E, A_S, A_N, A_B, and A_F are the contact areas among the elements. W_x, E_x, S_y, N_y, B_z, and F_z are the distances among the geometric center of the heat transfer elements.

$$\alpha = \frac{k}{\rho C}, \quad I_i = \frac{V_e}{A_i}, \quad i = E, B, N, W, F, S$$

5.2 *Boundary Element in the Rolling Region*

If no other heat loss is present besides the heat transfer and friction heat on the contact surface between the strip and the roller where the extra heat source is the same as the inside of the element, then the mathematical equation can be shown as (Ref 5):

$$KA_c \left(\frac{\partial T}{\partial n} \right)_b + K_R A_c \left(\frac{\partial T_R}{\partial n} \right) - \dot{q}_f = 0 \qquad \text{(Eq 10)}$$

where $(\partial/\partial n)_b$ represents the partial difference of the normal direction along the boundary. The subscript R represents the property related to the roller, whereas variables without the subscript R are related to the strip. To simplify the calculation, assume that the amount of friction heat transferred to the strip is (Ref 10):

$$\dot{q}_f' = \frac{\left(\frac{K}{\rho C} \right)^{1/2}}{\left(\frac{K}{\rho C} \right)^{1/2} + \left(\frac{K_R}{\rho_R C_R} \right)^{1/2}} \dot{q}_f \qquad \text{(Eq 11)}$$

In addition, assume that the heat conduction coefficient is $(K + K_R)/2$, then the amount of heat transfer along the element boundary in the rolling region is as follows. (a) the element is located on the upper surface of the strip:

$$\dot{q}_N = -\left(\frac{K + K_R}{2} \right) \frac{T_N^i - T_C^i}{N_y} A_N \qquad \text{(Eq 12)}$$

(b) the element is located on the lower surface of the strip:

$$\dot{q}_S = -\left(\frac{K + K_R}{2} \right) \frac{T_C^i - T_S^i}{S_y} A_S \qquad \text{(Eq 13)}$$

5.3 *Boundary Element in the Nonrolling Region*

On the contact surface between the heat transfer element and the exterior, since the boundary conditions are different, the amount of heat transfer consists of either one of the following two situations. The first situation is radiation heat loss and convection heat transfer of air:

$$\dot{q} = \left(S \varepsilon_m [(T_C^i + 273)^4 - (T_\infty + 273)^4] + h_{ar}(T_C^i - T_\infty) \right) A_c \qquad \text{(Eq 14)}$$

where h_{ar} is Stefan-Boltzmann constant, ε_m is surface emissivity, and T_∞ is room temperature (external temperature).

The second situation is film boiling heat transfer. The upper surface of the strip may be covered with cooling water. Since the working temperature is about 350 to 550 °C during hot rolling, which is much higher than the boiling point of the cooling water, the phenomenon of film boiling emerges. In this study, the experimental equation of Yamaguchi (Ref 11) is selected:

$$\dot{q} = (1.11)(1.163)(10^5)\dot{W}^{0.521} A_c \qquad \text{(Eq 15)}$$

where $\dot{W}$ is flow rate of cooling water [l/(min m^2)].

6. The Computer Program and Problem Statement

The program analysis of elasticity-plasticity is based on the increment theory, which uses a minute linear increment to approximate the deformation path. If an element falls between the elastic and plastic parameters, the Marcal method (Ref 12) for modifying the matrix $[D^{ep}]$ is used. In the solution of the large deformation and large strain problems, ULF(update lagrangain formulation) is used. Also, the construction of the equation uses the Jaumann rate of Euler stress to derive the overall rigid matrix. For the solution of juxtaposed one-order equations of the unsymmetrical matrix of Eq 4 and 5, the Cholesshy method (Ref 13, 14) is used. As for the heat conduction, the concepts of control volume and heat balance are utilized to analyze the transient heat transfer finite difference equation numerically.

In addition the strain hardening rate has to be modified to satisfy $|\bar{\sigma} - \sigma_{uni}| \div |\sigma_{uni}| \leq 5\%$. The value of time increment Δt has to be controlled to satisfy

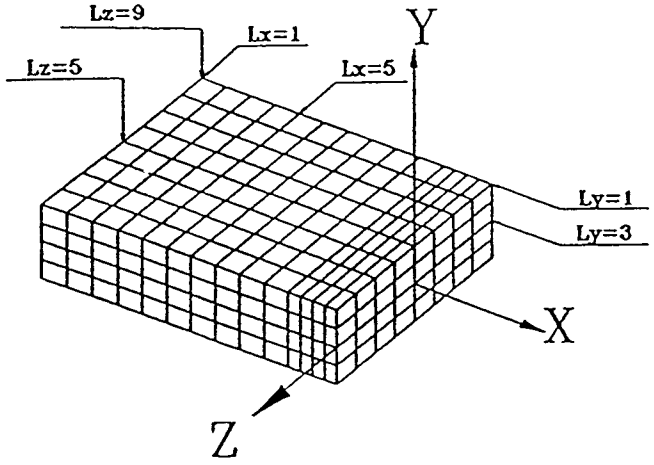

Fig. 4 Finite element mesh of the three-dimensional thermo-elastic-plastic strip for the simulation of hot rolling

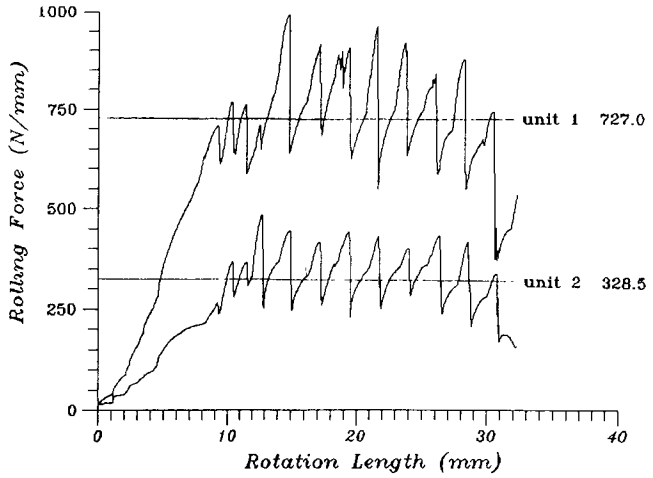

Fig. 5 History of rolling force of units 1 and 2

Table 1 Initial condition for the rolling simulation

Unit	Strip length, mm	Strip thickness, mm	Strip width, mm	Reduction ratio, %	Roller radius, mm		Roller rotation speed, rpm	
					Upper	Lower	Upper	Lower
1	25.10	6.27	18.82	14.17	79.38	79.38	19.20	19.20
2	25.10	6.27	18.82	14.17	79.38	79.38	19.20	19.20
3	25.10	6.27	18.82	14.17	79.38	79.38	19.24	19.20

$$e = \frac{|\Delta t[\dot{\bar{\varepsilon}}(t) - 2\dot{\bar{\varepsilon}}(t-\Delta t) + \dot{\bar{\varepsilon}}(t-2\Delta t)]|}{|\dot{\bar{\varepsilon}}(t)|}$$

In this article, $e \leq 0.005$ so as not to diffuse the equation. To ensure that the solution of Eq 9 can converge, therefore:

$$\Delta t < \left[\alpha\left(\frac{1}{I_E E_x} + \frac{1}{I_B B_z} + \frac{1}{I_N N_y} + \frac{1}{I_W W_x} + \frac{1}{I_F F_z} + \frac{1}{I_S S_y}\right)\right]^{-1}$$

For the initial condition of the rolling simulation and the finite element mesh of the strip, see Table 1 and 2 and Fig. 4. Unit 1 involves an isothermal symmetrical cold rolling at a temperature of 25 °C. Unit 2 is a nonisothermal symmetrical hot rolling, in which the initial temperature of the strip is 420 °C. The initial temperature of the roller is 40 °C. the cooling agent is water at a temperature of 40 °C. The heat transfer boundary conditions of unit 3, which involves a nonisothermal unsymmetrical hot rolling, are the same as those of unit 2. The rotation speed of the upper roller is 19.24 rpm, and that of the lower roller is 19.20 rpm. The cross section and series number of Lx, Ly, and Lz of the strip as shown in Fig. 4 were introduced first to facilitate the analysis of results. The simulation conditions in Tables 1 and 2 are taken as the Al-Salehi experimental condition (Ref 8) for cold rolling. Unit 1 of symmetric cold rolling is conducted to simulate the Al-Salehi experimental results.

The Tseng (Ref 5) experiment data were chosen as the material properties of aluminum strip. For aluminum strips of 99.6% purity, its effective stress is shown as the function of strain, strain rate, and temperature as:

$$\bar{\sigma} = A(\theta)B(\theta)\bar{\varepsilon}^{n(\theta)}\left[\frac{\dot{\bar{\varepsilon}}}{5\times 10^4}\exp\left(\frac{1.436}{8\times 10^{-5}\times 933\times\theta}\right)\right]^{m(\theta)}$$

where,

$\bar{\sigma}$ = effective stress

$$\theta = \frac{T}{T_m}$$

T = strip temperature, K

T_m = melting point of aluminum strips, 993 K

$A(\theta) = 100 \times [1 - (\theta - 0.08) \times \exp(1 - \theta)]$

$B(\theta) = 3^{0.5\times[1 + n(\theta) + m(\theta)]}$

$0.0 < \theta \leq 0.54716,\ m(\theta) = 0.055980$

$0.54716 < \theta \leq 1.0,\ m(\theta) = 0.336\,(\theta - 0.456)$

$$n(\theta) = 0.5 \times \left\{1 - \theta \times \exp\left[0.5535\left(1 - \frac{1}{\theta}\right)\right]\right\}$$

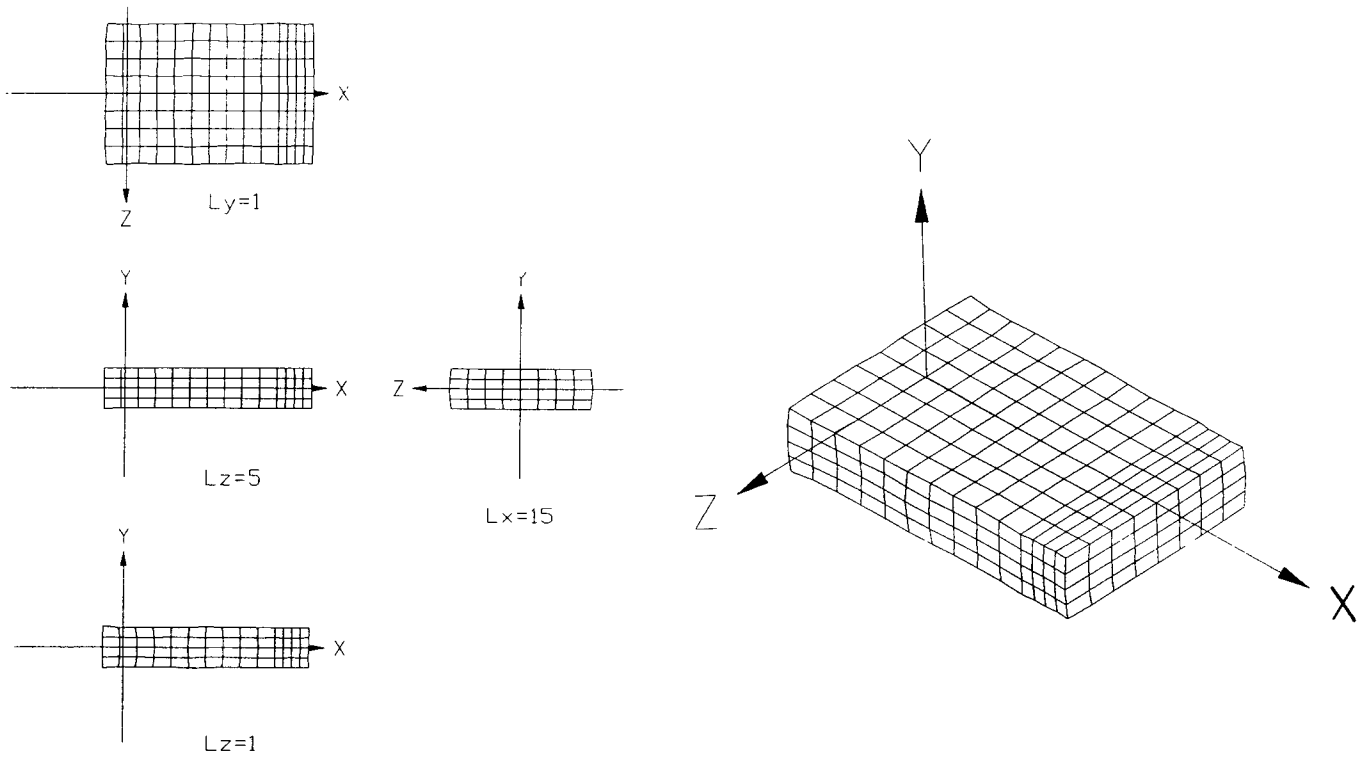

Fig. 6 Three-dimensional strip shape of unit 1 at final steady state

Table 2 Input data of the rolling simulation

Unit	Initial ΔD, mm	Initial temperature of the strip, °C	Initial temperature of the roller, °C	Room temperature, °C
1	0.018	25	25	25
2 and 3	0.018	420	40	25

The other material properties of aluminum strip are as follows:

Young's modulus = 68.5 GPa

Poisson's ratio = 0.33

Linear expansion coefficient = 3.2×10^{-5}/°C

Heat-transfer coefficient (k_s) = 0.22 W/mm^2 °C

Density (ρ_s) = 2.6 g/cm^3

Specific heat (c_s) = 1.13 J/g °C

Air heat transfer coefficient (h_{as}) = 2×10^{-5} W/mm^2 °C

Surface emissivity (ε_m) = 0.2

Efficiency of deformation energy transformed into thermal energy (η_p) = 0.95

7. Results and Discussion

This study developed the three-dimensional coupled thermo-elastic-plastic finite element model of nonisothermal rolling and analyzed the curvature of aluminum strips caused by the difference in the heat transfer boundary conditions of the upper and lower rollers. The difference in the rotation speed between the upper and lower rollers was utilized in an attempt to correct the aforementioned curvature in hot rolling due to unsymmetrical heat transfer boundary conditions. In addition, the changes in shape, temperature field, and strain field of the strip during the various stages were analyzed and can be used to obtain the lateral plastic flow of the strip.

To verify the justification of the three-dimensional coupled thermo-elastic-plastic finite element model of unsymmetrical rolling derived in this study, a unit of cold rolling simulation was conducted. The obtained rolling force was then compared with the experimental data of rolling force from published studies. The first unit involves the cold rolling of an aluminum strip

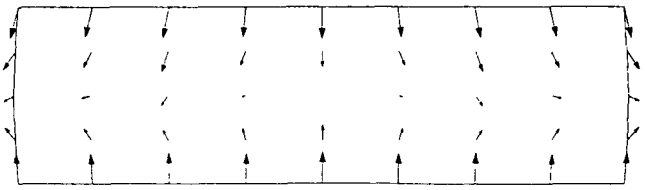

Fig. 7 Displacement of the cross section (Lx = 8) of unit 2 at middle steady state

Table 3 Rolling torque of unit 1 of cold rolling compared with the experimental data of Ref 8

Source	Rolling torque, N-mm/mm	Difference rate, %
Torque meter	1944	18.1
Integrated experimental results	2291	0.22
Calculated (Bland and Ford)	2345	–2
This work	2296	0

Difference rate is the rolling torque of this paper minus the experimental data divided by the rolling torque of this paper.

Table 4 Average rolling force of the three units

	Average rolling force, N/mm			
Unit	Upper roller	Lower roller	Aggregate	Difference
1	727.0	727.1	727.0	0.1
2	325	332	328.5	7
3	344.4	344.6	344.5	0.2

Difference is rolling force of lower roller minus rolling force of upper roller.

under an isothermal state. Figure 5 shows the history of rolling force. The average rolling force is 727 N/mm. The experimental data from the Al-Salehi (Ref 8) study is 696 N/mm. Therefore, the difference is only 31 N/mm, or a mere 4.5%, which can be seen as an acceptable calculation error. This indicates that the results in this study are accurate. In addition, the rolling torque is compared with the experimental data. The average rolling torque of the first unit of cold rolling is 2296 N-mm/mm. The experimental values reported by Al-Salehi (Ref 8) are 1944 N-mm/mm for torque meter, 2291 N-mm mm for integrated experimental results, and 2345 N/mm/mm for calculated (Bland and Ford). Results indicate that the simulated values in this paper fall in the range of experimental values. The differences are listed in Table 3. Li and Kobayashi (Ref 1) used the rigid plastic finite element method to solve the plane-strain rolling problem. The average rolling torque derived from the numerical simulation analysis is approximately 3000 N-mm/mm, which verifies the feasibility of this paper.

Table 4 lists the average rolling force of the upper and lower rollers and the aggregate average rolling force of each unit. The difference in the average rolling force of the upper and lower rollers (the average rolling force of the lower roller subtracted by that of the upper roller) is also listed in Table 4. Since the

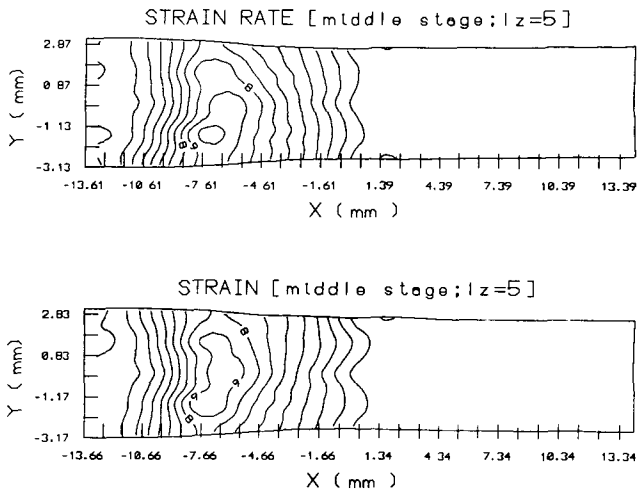

Fig. 8 Strain rate of Lz = 5 plane of units 2 and 3

cold rolling conditions are completely symmetric in unit 1, the difference between the average rolling forces of the upper and lower rollers approaches zero. Unit 2 is nonisothermal hot rolling, with an aggregate average rolling force of 328.5 N/mm, which is only 45.2% of the aggregate average rolling force of unit 1, and with a aggregate average rolling torque of 1253 N-mm/mm, which is only 54.6% of the aggregate average rolling torque of unit 1. Results indicate that hot rolling can greatly reduce the rolling force and the rolling torque. Further, there is a difference of 7 N/mm in the average rolling forces of the upper and lower rollers in the simulation due to unsymmetrical heat transfer boundary conditions. Unit 3 is the nonisothermal and unsymmetrical hot rolling with different roller speeds. The difference in the rotation speed was used to correct the effects caused by the difference in heat transfer boundary conditions. The aggregate average rolling force is 344.5 N/mm, which is 16 N/mm more than that of unit 2. This increase indicates that the difference in the rotation speed of rollers will result in an increase in rolling force. But the difference in the rolling forces of the upper and lower rollers is close to zero. In terms of the analysis of rolling force, unit 3 can effectively correct the unsymmetrical difference caused by unit 2, but will result in the increase of the aggregate average rolling force.

Figure 6 is the three-dimensional strip shape of unit 1 at the end of the steady state. The upper and lower surfaces (Ly = 1) of the strip extended sideways by about 1.2% at the final stage of rolling, whereas the central surface (Ly = 3) extended sideways by about 3.1%. Compared with the experiment by Lahoti et al. (Ref 15), in which the average sideways extension is 2% under the conditions of width-height (W/H) = 3 and reduction ratio = 15%, these results are still reasonable. Figure 6 shows that there is the phenomenon of bulge at both sides of the strip exit, while there is a dent at the front end close to the two sides. There is also a bulge at the center end because the easy plastic flow on the upper and lower surface of the strip resulted from the lack of restriction from the roller friction on the two sides of the strip near the front end. As for the center front end, since it is a free end, the phenomenon of bulge is natural during plastic deformation.

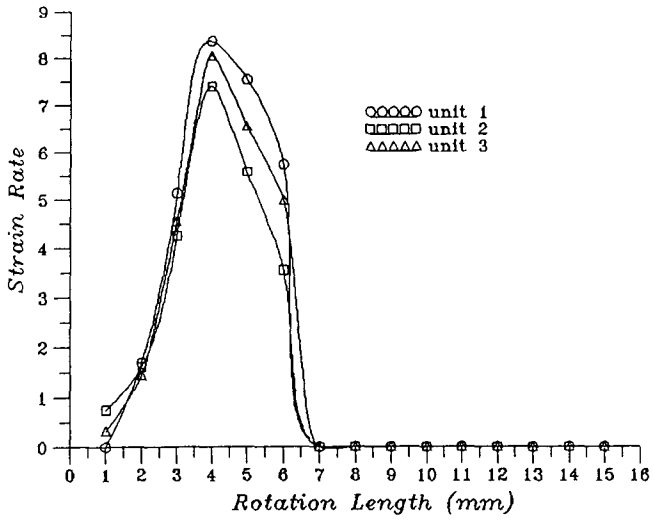

Fig. 9 Comparison of strain rate of the three units on the Ly = 3 and Lz = 5 plane

Figure 7 shows the displacement of the cross section (Lx = 8) of unit 2 when the rolling reached the middle steady stage. Figure 7 indicates the lateral plastic flow of the strip during rolling, which provides a better understanding of the bulge phenomenon.

Unit 2 involves nonisothermal hot rolling. The function of the coolant resulted in unsymmetrical heat transfer conditions, which in turn caused vertical curvature. The curvature deviates 0.6 mm upward from the center line. In unit 3, a difference in the rotation speed of the rollers was used to correct the strip shape. The rotation speed of the upper roller was set at 19.24 rpm, and that of the lower roller was set at 19.2 rpm. Figure 8 shows that the resulting center line of the strip was almost horizontal, which proves that the strip curvature caused by nonisothermal rolling can be corrected by adjusting the rotation speed of the upper and lower rollers.

Since the theoretical model in this study assumes the strip to be thermo-elastic-plastic, the area with a strain rate slightly larger than zero is the plastic deformation zone. Hence, from Fig. 8, the plastic deformation zone roughly starts before the entrance and ends at the exit. However, whether in cold rolling or hot rolling, the highest strain rate occurred at the surface within the rolling area near the entrance. The connective line is divided at the neutral point. Between the entrance point and the neutral point, the curve bends toward the entrance point. Between the neutral point and the exit, the curve bends toward the exit point. Figure 9 shows that the order of the strain rate value is unit 1, unit 3, and unit 2. Results indicate that a larger strain rate occurs during cold rolling; hot rolling tends to yield a smaller strain rate due to the easy plastic flow of metals. But the value of strain rate increases in unsymmetrical hot rolling. Hot rolling also causes plastic deformation to occur earlier.

In Fig. 9, the strain rate of unit 1 still stands at zero at point one, while those of units 2 and 3 have obviously gone beyond that. The strain rate of the node of strip close to the entrance point shows a steep increase. The strain rate reaches the highest value near the entrance and then declines very quickly afterward.

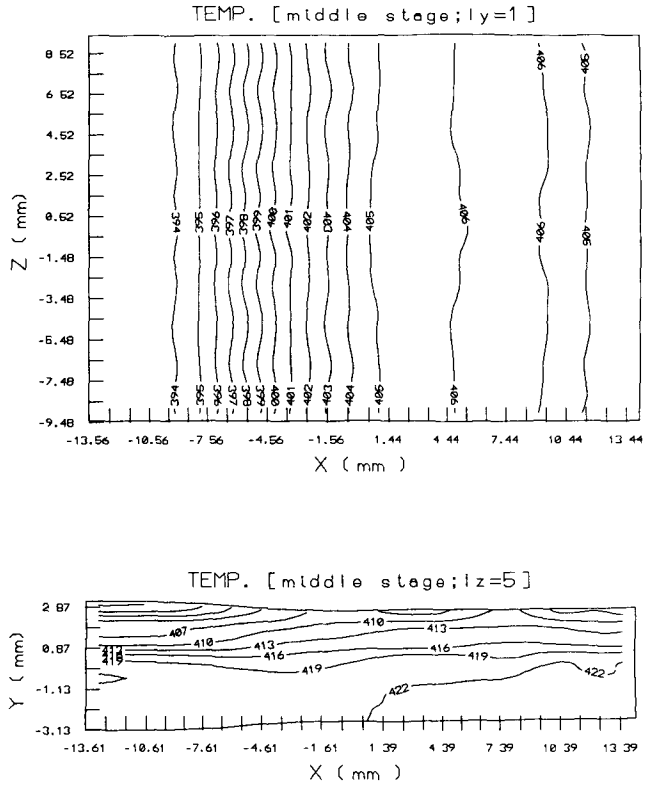

Fig. 10 Temperature distribution of Ly = 3 and Lz = 1 plane of unit 2 with middle stage

Figure 10 shows the temperature distribution of the Ly = 3 and Lz = 1 cross section of unit 2. The temperature at the center portion before the entrance point is higher because between the neutral point and entrance point, the strip moves toward the entrance point, resulting in higher temperatures at portions close to the sides. Between the neutral point and the exit point, the plastic flow of the strip moves toward the direction of the exit point. As a result, the higher temperature occurs at the center portion of the strip. In addition, since there are no experimental data on temperature distribution available in related studies, results are compared with the simulation analysis by Dawson (Ref 16), as shown in Fig. 5. Reference 16 records the same distribution trend, and the temperature contours are approximately parallel to the roll surface, indicating an overall heat flux in the direction of the roll. The feasibility of this paper is thus verified. Further, the difference in heat transfer boundary conditions causes the unsymmetrical temperature distribution on the upper and lower surfaces of the strip, with a temperature difference between the two surfaces reaching 30 °C. The difference in temperature is entirely determined by the heat transfer boundary conditions. In unit 3, the difference in the rotation speed of the upper and lower rollers also causes unsymmetrical temperature fields of the upper and lower surfaces of the strip. The greater rotation speed of the lower roller results in a relatively greater displacement of the lower surface. This causes an increase in stress and strain, which in turn produces a greater plastic deformation heat and friction heat. The value derived from heat transfer has a smaller effect and thus becomes less distinct in hot rolling.

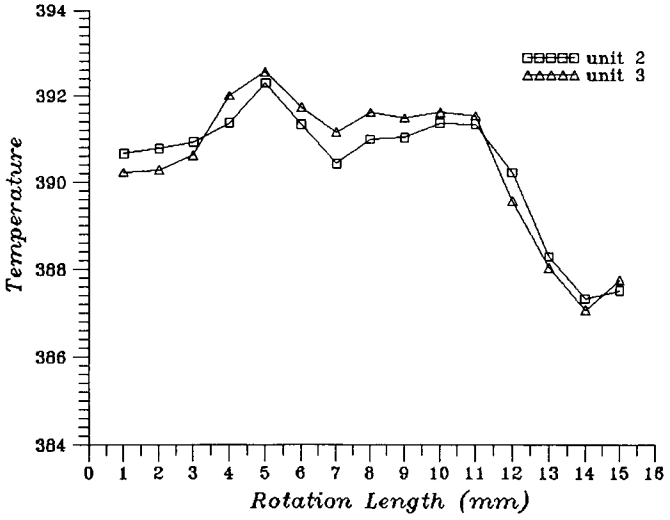

Fig. 11 Comparison between the temperature on Ly = 3 and Lz = 5 plane for units 2 and 3

Figure 11 compares the temperatures on the Ly = 3 and Lz = 5 cross sections. It shows that the temperatures of units 2 and 3 are almost the same, which indicates that the major changes in heat in hot rolling come from heat transfer.

8. Conclusions

This study successfully developed the finite element model of the three-dimensional coupled thermo-elastic-plastic rolling. The transfer boundary conditions in an actual rolling were completely considered by the transient finite difference method to obtain the temperature field of the strip and analyze the non-isothermal rolling phenomenon. A cold rolling simulation was also conducted using this model. Results indicate that the size and distribution of the rolling force and the rolling torque compared with the experimental data obtained by Al-Salehi (Ref 8) are reasonable. There were bulges on the front and rear ends and both sides of the strip at the final stage of rolling. Compared with the experiment by Lahoti et al. (Ref 15), the theoretical model and computer program developed in this study are reasonable. In addition, we analyzed the effects of unsymmetrical heat transfer boundary conditions on the strip. Finally, a difference in the rotation speed of rollers was used to correct the effects of unsymmetrical heat transfer boundary conditions. The following important conclusions were drawn in this study.

Hot rolling can greatly reduce the rolling force. Unsymmetrical heat transfer boundary conditions will cause unsymmetrical rolling forces of the upper and lower rollers. However, the above condition can be corrected by the difference in the rotation speed of the rollers. This correction can achieve the symmetrical distribution of the rolling force and result in an increase of the aggregate average rolling force.

In this study, the rotation speed of the upper roller was set at 19.24 rpm, and that of the lower roller was set at 19.20 rpm to successfully correct the strip curvature due to unsymmetrical heat transfer boundary conditions. The displacement of the various points of the strip also offers some insight into the plastic flow of the strip during rolling.

The easy flow of metals during hot rolling results in an early appearance of plastic deformation and a smaller strain rate. The difference in the rotation speeds of the roller will produce a considerable increase of the strain rate.

The distribution of temperature field is greatly affected by the heat transfer boundary conditions. For example, in unit 2, the difference between the temperatures of the upper and lower surfaces of the strip is as high as 30 °C. The impact of the difference in roller rotation speeds on plastic deformation rate and the friction heat is not very impressive compared with that of heat transfer boundary conditions. In other words, there is not much difference between the temperature fields of units 2 and 3.

References

1. G.-J. Li and S. Kobayashi, Rigid-Plastic Finite-Element Analysis of Plane Strain Rolling, *J. Eng. Ind.*, Vol 104, 1982, p 55-64
2. R. Shivpuri, P.C. Chou, and A.C.W. Lau, Finite Element Investigation of Curling in Non-Symmetric Rolling of Flat Stock, *Int. J. Mech. Sci.*, 1988, p 625-635
3. B.K. Chen, S.K. Choi, and P.F. Thomson, Analysis of Plane Strain Rolling by the Dynamic Relaxation Method, *Int. J. Mech. Sci.*, Vol 31, 1989, p 839-851
4. O.C. Zienkiewicz, E. Onate, and J.C. Heinrich, A General Formulation for Coupled Thermal Flow of Metal Using Finite Elements, *Int. J. Numer. Methods Eng.*, Vol 17, 1981, p 1497-1514
5. A.A. Tseng, Finite Difference Solution for Heat Transfer in a Roll Rotating at High Speed, *Numer. Heat Transfer*, Vol 17, 1984, p 113-125
6. A.A. Tseng, A Numerical Heat Transfer Analysis of Strip Rolling, *ASME J. Heat Transfer*, Vol 106, 1984, p 512-517
7. C. Devadas and I.V. Samarasekera, Heat Transfer during Hot Rolling of Steel Strip, *Ironmaking and Steelmaking*, Vol 13 (No. 6), 1986, p 311-321
8. F.A.R. Al-Salehi, T.C. Firbank, and P.R. Lancaster, An Experimental Determination of the Roll Pressure Distributions in Cold Rolling, *Int. J. Mech. Sci.*, Vol 15, 1973, p 693-710
9. Z.C. Lin and S.Y. Lin, An Investigation of a Coupled Analysis of a Thermo-Elastic-Plastic Model during Warm Upsetting, *Int. J. Mach. Tools Manuf.*, Vol 30 (No. 4), 1990, p 599-612
10. Z.C. Lin and C.J. Lee, A Coupled Analysis of the Thermo-Elastic-Plastic Large Deformation for Upsetting Process, *J. Chin. Soc. Mech. Eng.*, Vol 10 (No. 3), 1989, p 197-209
11. Y. Yamaguchi, M. Nakao, K. Takatsuka, S. Murakami, and ?. Hirata, *Nippon Steel Tech. Rep.*, Vol 33 (No. 4), 1985
12. P.V. Marcal and I.P. King, Elastic-Plastic Analysis of Two Dimensional Stress System by the Finite Element Method, *Int. J. Mech. Sci.*, Vol 9, 1967, p 143-155
13. C.F. Gerald and P.O. Wheatley, *Applied Numerical Analysis*, 3rd ed., Addison-Wesley, 1984
14. K.J. Bathe, *Finite Element Procedures in Engineering Analysis*, Prentice-Hall, 1982
15. G.D. Lahoti, N. Akgerman, S.I. Oh, and T. Altan, Computer-Aided Analysis of Metal Flow and Stresses in Flat Rolling, *J. Mech. Work. Technol.*, Vol 4, 1980, p 105-119
16. P.R. Dawson, On Modeling of Mechanical Property Changes during Flat Rolling of Aluminum, *Int. J. Solids Struct.*, Vol 23 (No. 7), 1987, p 947-968